TRANSITION MEASUREMENT SYSTEM OF EXPERIMENTAL SUPERSONIC TRANSPORT "NEXST-1"

Naoko Tokugawa *, Dong-Youn Kwak*, and Kenji Yoshida *
***Japan Aerospace Exploration Agency**

Keywords: *Boundary Layer, Transition Measurements, Supersonic Transport, Natural Laminar Flow, Flight Test*

Abstract

Flight test of an unmanned and scaled supersonic experimental airplane "NEXST-1" is performed by Japan Aerospace Exploration Agency, to validate CFD-based aerodynamic design. The natural laminar flow wing concept as the most original design is validate by measuring the surface pressure and the transition location. Therefore high quality transition measurement system is constructed to detect transition location. The transition location detected experimentally is in good agreement with numerically predicted location, and the natural laminar flow effect is confirmed at the design condition.

1 Introduction

1.1 Outline of "NEXST" program

A great number of technical problems remain to make the next generation supersonic transport flyable. The problems are reduction of the fuel consumption and sonic boom, improvement of the aerodynamic performance, suppression of aerodynamic noise at the taking off and landing, compromise of aerodynamics and structures, environmental protection and so on. The drag reduction is one of the most important problems among them. Therefore in Japan Aerospace EXploration Agency (JAXA), "National EXperimental Supersonic Transport (NEXST)" program [1,2] has been promoted to develop a CFD-based aerodynamic design technology for designing the body of the low drag with high fuel efficiency.

1.2 Aerodynamic Design of Natural Laminar Flow Wing

Four aerodynamic design concepts are applied to realize the low drag of the body [3]. Those are warped wing [4] and the arrow planform [5] for reduction of the lift-dependent drag, the area-ruled body [6] for reduction of the wave drag due to volume and the Natural Laminar Flow (NFL) concept for reduce the friction drag [3,7,8]. NLF concept, which is applied to the upper surface of the main wing, is the most original design. Because it used be believed that the natural laminarization on the swept wing with subsonic leading edge, which is employed for the reduction of the lift-dependent drag, can not be achieved at the supersonic speed, due to the cross-flow instability which leads the early boundary layer transition at the leading edge region. But in this project, NFL concept is applied as the first challenge in the world, based on the recent development of CFD technology and transition prediction method. The boundary layer transition on the 3-D wing is generally known to be governed by cross-flow instability in the leading edge region. And, in the following adverse pressure gradient region, T-S wave type instability will grow. But we expect that the NFL effect can be obtained based on two ideas for pressure gradient as follows: one is the minimization of the distance between the leading edge and suction peak to suppress the growth of cross-flow instability, and the other is the negligible adverse pressure gradient after the suction peak to suppress the T-S wave type instability. To obtain a wing section achieving

the surface pressure distribution as a design target, we developed a CFD-based "inverse" design method [9]. The inverse design method is a method to obtain the wing section through the iterating modification of the wing section to make its surface pressure distribution coincident with the target optimum pressure distribution. The transition location on the upper surface of the designed wing is predicted by the e^N-method using a numerical code so called "LSTAB" originally developed in JAXA, which is based on the linear stability theory in the 3-D compressible boundary layer [10-12]. The transition location predicted by LSTAB is expected to be much backward location such as 45~60%C at the design point with lift coefficient of full configuration C_L=0.10, though it moved much forward on the condition except for the design point. Therefore, it expects to obtain the NLF effect on the designed wing. The NFL effect on the wing designed by inverse design method has been validated by means of a wind tunnel test using a wing-body configuration model [13,14]. However the freestream disturbance in usual supersonic tunnels is relatively larger than flight condition and the unit Reynolds number is lower. Thus the aerodynamic design concept must be validated in flight. Therefore, JAXA conducted a flight test by use of an unmanned and scaled supersonic experimental airplane. It was the first attempt to measure the boundary layer transition in the supersonic flight test in Japan.

1.3 Supersonic Experimental Airplane NEXST-1 and Flight Experiment

The supersonic experimental airplane, which is called "NEXST-1", is a vehicle of total length 11.500m, full span 4.718m and total weight including all components is 1940.7kg [3,15]. The wing and the nose surface was polished up to below 0.3μm in arithmetical mean deviation, as same level as a transition model for wind tunnel testing, since external disturbances which can lead to transition must be excluded.

This flight experiment was successfully conducted at the Woomera Prohibited Area (WPA) in South Australia. The NEXST-1 was launched on October 10, 2005, by the solid rocket booster in piggy-back form as shown in Fig. 1 [15]. After the separation from the rocket booster at an altitude of H≈19km, the NEXST-1 flied at supersonic speed like a glider through two successive test phases. During the flight more than 500 technical data, such as aerodynamic performance, surface pressure [16,17] and boundary layer transition, was acquired at Mach number M≈2. After the experimental flight, the NEXST-1 was recovered on the ground by use of parachutes and airbags.

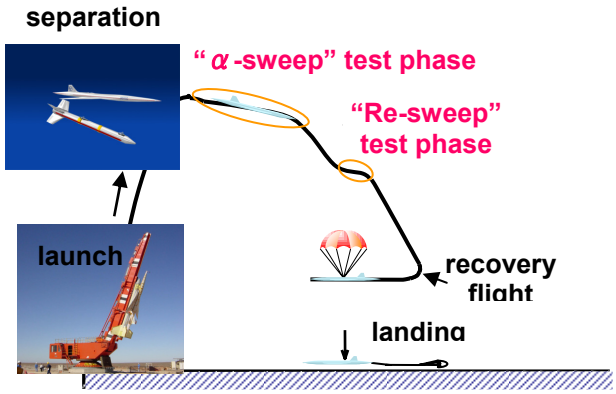

Fig. 1. Outline of the flight test of supersonic experimental airplane NEXST-1.

The first of the two test phases is called "α–sweep" test phase, in which the angle of attack α was controlled to take six values for specific lift coefficient C_L including the design point [15]. At the 4th step, the lift coefficient had the design value C_L=0.10. The angle of attach was held during about 4 seconds in each step because of the requirement on the pressure measurement system [16,17]. After the α–sweep test phase, the NEXST-1 was descended rapidly to recover a Mach number, then entered into the second test phase. The second test phase is called "Re–sweep" test phase, in which NEXST-1 glided in keeping a constant lift coefficient at the design point (C_L=0.10). The variation of Reynolds number Re_c based on the mean aerodynamic chord (MAC) at the Re-sweep test phase was from 34.7×10^6 to 36.9×10^6, and therefore it was not significant because of a shorter flight time than that of our estimation.

The largest variation of Re_c, however, was obtained when the Re_c values between the Re–sweep test phase and the 4th step of the α–sweep test phase were compared. The Reynolds number at the 4th step of the α–sweep test phase, $Re_c=14.0\times10^6$ was one third of that at the Re–sweep test phase.

1.4 Purpose

The purpose of this paper is to present the transition measurement system of the NEXST-1. In this paper, the transition measurement system is introduced, with the examinations of its function through preliminary tests on the ground. These tests are necessary for the present system, since transition measurement in flight by using this system is the first challenge, and we have only one chance of the flight test. At last, the results of the transition measurement obtained in the flight test are also summarized.

2 Transition Measurement Systems

2.1 Outline

Four types of sensors which were used to detect the transition location in the NEXST-1 experimental airplane were hot-film sensor (HF), dynamic pressure transducer (DP), thermocouple (TMP), and Preston tube (Pr).

These sensors were mainly distributed in arrays of spanwise position normalized semi-span length $Y/S\approx0.3$, 0.5, 0.7 for the left wing (Fig. 2), and on the left side of the nose. The reason why the left side was mainly used for transition measurement was that any turbulence in the right wing and right side of the nose areas was supposed to occur caused by the air data sensor, which protrudes from the right side of the nose. These sensors were installed on the surface of the NEXST-1 airplane with a permitted step of less than 40μm and were arranged at an inclination of 15~20° on the wing side to the flow direction so that the upstream sensor does not disturb the downstream boundary layer (Fig. 2). The three kinds of sensors expect to the Preston tube were arranged to supplement each other in a row. Although Preston tube was arranged separately from other three flash mounted sensors, as it becomes considerable surface roughness and disturbs downstream boundary layer (Fig. 2). On the other hand, each sensor was shifted 10° or 15° in a circumferential direction on the nose. In general, inflow and outflow at the gap between the sensor and the body can disturb the boundary layer and promote the transition. Therefore, the sealant was thickened around the sensor inside of the body to prevent leaks. Moreover it was confirmed that there were no leaks as pressure was absorbed at the gap between the sensor and the body.

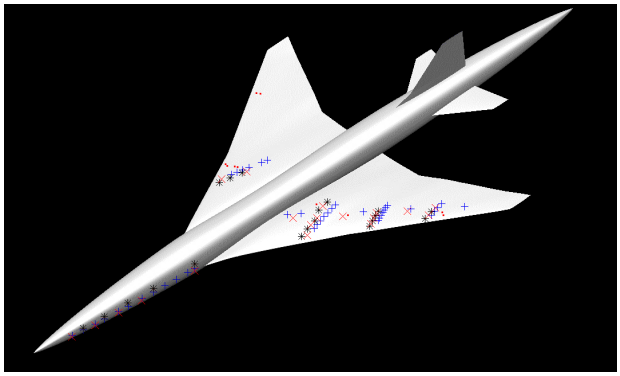

Fig. 2. Sensor position. Pink "×", black "*", blue"+" and red "•" correspond to HF, DP, TMP and Preston tube, respectively.

2.2 Hot-film sensor and Dynamic Pressure Transducer

The hot-film measures surface shear stress and its fluctuation. The sensor was equivalent to the DANTEC 55R45, but was a custom-made item with an L-shaped which is suitable to mount on the thin leading edge. It was operated by the constant temperature anemometer (CTA), which is called signal conditioner #1. This was custom-developed for this experimental airplane (by Kyowa Electronic Instruments Co. Ltd.,) at overheat temperate 220°C. The CTA was designed to begin supplying bridge power when the experimental aircraft separated from the rocket at its highest altitude, so that the sensor would never be destroyed by rapid environmental temperature variations on launch. To sense high frequency fluctuations accurately,

AC outputs over 10Hz and under 10kHz were separated from DC outputs under 100Hz, and amplified with 60 times gain. This AC gain was determined based on the estimation of the flight data through the wind tunnel test as described below. Electrical noise is reduced to about $1mV_{RMS}$.

The dynamic pressure transducer measures surface pressure and its fluctuation with high frequency response as well as HF. The transducer was a semiconductor strain gauge type (Kulite Corp. XB44-093), and a 0.7BAR-differential type. The pressure amplifier to operate this pressure transducer was also custom-developed by Kyowa, which is called signal conditioner #2. The output was separated in DC outputs under 100 Hz, and AC outputs over 10 Hz and under 10 kHz, which is similar to the HF output. The DC and AC output are amplified with a 140 and 100 times gain, respectively. The DC gain of DP was also determined based on the estimation of the flight data through the wind tunnel test as described below. Electrical noise was reduced to about $6.7Pa_{RMS}$.

For both signal conditioners, cross talk was reduced to -40dB. DC-DC converter included in the signal conditioners was designed robust to prevent from some abnormal working of power supplier such as instantaneous cut off. A low-pass filter with cut-off frequency 10kHz was included at the AC output of both signal conditioners to avoid aliasing. Offset of AC outputs were monitored.

The DC and AC outputs were pulse code modulated by signal processors. They are then recorded in the data recorders with 12bit, 250 Hz sampling for the DC output, and 10bit, 20 kHz sampling for the AC output. The DC output is also transmitted to the control center so called “Instrumentation building” using a telemeter system.

2.3 Thermocouple

In general, properties of the heat transfer by convection depend on the flow conditions. It means that the heat transfer coefficient on the laminar flow is different from that on the turbulent flow. The differences of the heat transfer coefficient of the flow induce the different temperature variation with time on the wall. Thus, the thermocouple is one of the desirable tools to detect the boundary layer transition locations, because the temperature variation on the airplane surface has different behaviors when the flow is laminar or the turbulence. Type-K and un-grounded coaxial thermocouples (Okazaki Manufacturing Co.) were mounted on the NEXST-1 (Fig.2). Zero point reference box was also equipped on the fuselage. To prevent the electric and magnetic noise from the signal cable, double shielded cables were used on most part of the signal lines. Measured analog data were amplified and converted to digital data by a signal processor.

2.4 Preston tube

Ten Preston tubes were mounted on the upper surface of the wing (Fig.2). As well known, the velocity profile on the laminar boundary layer is different from that on the turbulent boundary layer. Since Preston tube measures a local total pressure near the surface, measured total pressure is different from flow conditions. Therefore, Preston tube can detect the boundary layer transition locations. The cross section of Preston tube tip is rounding rectangular with 0.15mm height and 1.15mm width. The pressure measurement system for Preston tube is same with a system for surface pressure measurement that was detail described in the references 16 and 17.

3 Preliminary Ground Test

3.1 Wind Tunnel Test

A wind tunnel test was performed to confirm the function of transition measurement system and to estimation of the data obtained in the flight test. To achieve the purpose, the same sensors and amplifiers as those actually mounted on the NEXST-1 were used in the wind tunnel test. Although, the gain in AC output of the CTA was 20 times (60 times on

the NEXST-1), and the gain in DC output of the pressure amplifier was 350 times (140 times on the NEXST-1). The wind tunnel test was conducted at High Speed Wind Tunnel of Fuji Heavy Industries, Ltd., which was in-draft type. This wind tunnel was suitable for this type of test because the unit Reynolds number is comparatively close to the flight condition of unit Reynolds number Re/m=12.3×10^6 at M=2.0, and the pressure fluctuation in the uniform flow was very low at Cp_{RMS}=0.4%. The model consisted of the front part of a Sears-Haack body ($y = f_{nose}(x) = A[x/l(1-x/l)]^{3/4}$, where $l = 2692.308$ and $A = 217.59$) which is the same shape as the nose of the NEXST-1. Although four kinds of sensors were flush mounted at X_{tip}=250mm from the tip and with a 60° spacing in the circumference direction, the results shown below was obtained at the condition with each sensor placed on the top line by rotating the model in the circumference direction. Since the locations of the sensors were fixed on the model surface and the total pressure of the wind tunnel was uncontrollable at almost atmospheric value, the transition location was detected by means of the continuous variation in angle of attack.

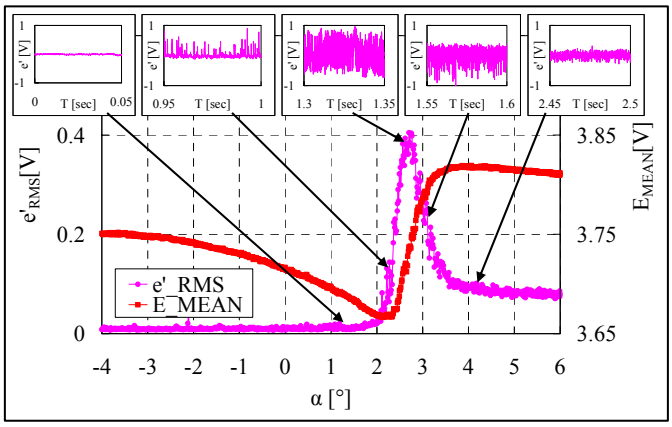

Fig. 3. Variation of HF DC and AC outputs with angle of attack, and corresponding time traces on the top line of the Sears-Haack body measured in the wind tunnel test.

The result is explained in the following. First of all, the variation in average of HF DC output E_{MEAN} and the fluctuation in HF AC output e' with the angle of attack are shown in Fig. 3. As is clearly shown in this figure, the average of HF DC output decreased gradually and increased rapidly like almost stepwise with the angle of attack. Since the variation in HF DC output corresponds to the variation in wall shear stress on the boundary layer from laminar to turbulent, as already mentioned, low average of DC output corresponds to low wall shear stress on the laminar boundary layer. On the other hand, high average shows the boundary layer is turbulent with high wall shear stress. Therefore, the stepwise increasing in HF DC output corresponds to the laminar-to-turbulent transition of the boundary layer. Meanwhile, the fluctuation in HF AC output also varied corresponding to variations in DC output. The amplitude of fluctuations in AC output was very small before the DC output begins to grow, and it was moderate after the DC output reaches to high value, furthermore it was at a maximum between these two states. Since the fluctuation in AC output is known to be small at the laminar state and larger at the turbulent, the state of the boundary layer is easily estimated from the fluctuation in AC output. It corresponds to that estimated from the average of DC output. The variation of AC output, however, shows the earlier onset and later end of transition than those detected from the DC output; the fluctuation in AC output tends to detect the boundary layer transition more sensitively. By the way, the variation in fluctuations in the HF AC output, taking a maximum between laminar and turbulent states, is caused by typical variations in instantaneous time traces, and it does seem to relate to the occurrence of turbulent spots (Fig. 3). At the beginning of the transition process, the fluctuation in HF AC output increased corresponding to the occurrence of the positive spike signal in the time trace. This could be caused by an instantaneous increase in DC output in line with the passage of turbulent spots. As the transition process progresses, and as turbulent spots occur more frequently, the fluctuations in AC output increased. After the peak of the fluctuation, the local laminar region is remained in turbulent boundary layer, and then negative spike signals seemed to occur. Such variations in the fluctuation and time trace of the HF AC output were observed not only on the transition in the compressive boundary layer,

but also in the low subsonic flow [18,19]. These values are expected to help in clarifying the boundary layer state in transition detection, acting as an effective guidepost.

The fluctuations in DP AC output *p'* with the angle of attack, similar to the HF AC output, are plotted in Fig. 4. The angle of attack where the fluctuation is at maximum condition also agrees with the maximum HF condition. The variation in instantaneous time trace is also found to be similar to the HF output. While the upward or downward spike signal was not as significant as the HF AC signal, the characteristic of skewness, which is positive at the beginning of the transition and negative at the end, is the same. Therefore, the variation in the time trace of the DP AC output is also regarded as being a significant guidepost for detecting the transition.

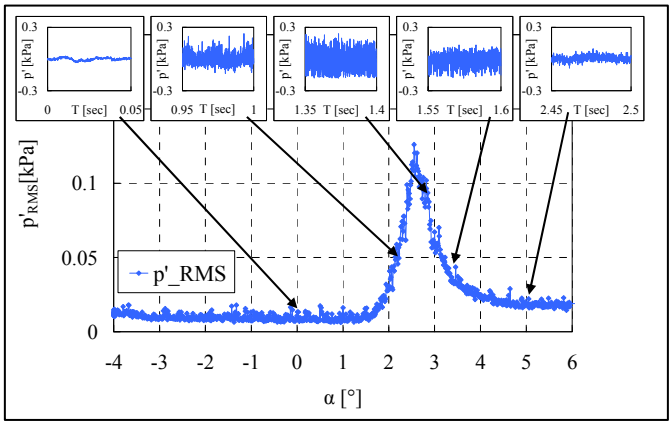

Fig. 4. Variation of DP AC output with angle of attack, and corresponding time traces on the top line of the Sears-Haack body measured in the wind tunnel test.

Time trace of the surface temperature T_{TMP} measured by the thermocouple are shown in Fig.5. In the case of α-sweep (the angles of attack increase continuously from –4° to 6°), time trace of temperature and corresponding variation on angle of attack α are shown in red and pink line respectively. In this case, the temperature gradient has a constant value until T=6 seconds, and then the gradient changes to another value. The angle of attack, which corresponds to the change of the temperature gradient, is α=2.8°. The time trace of the temperature in the case of α-constant (α =0° and 5°) were also plotted in Fig.5. The temperature gradient on α=0° (black line) corresponded with that observed at α<2.8° of α -sweep case. Similar tendency was observed on α=5° (blue line) and α>2.8° of α-sweep case. It means that gradual temperature gradient observed at α<2.8° was induced by the laminar flow, on the other hand, steep gradient observed at α>2.8° was induced by the turbulent flow when the α-sweep case. Higher heat transfer coefficient on turbulent flow induces higher gradient of temperature as compared with the laminar flow that has lower heat transfer coefficient. The detection of the boundary layer transition locations on the flight test by means of the thermocouple was confirmed from the wind tunnel test that simulated the α-sweep phase on the flight test.

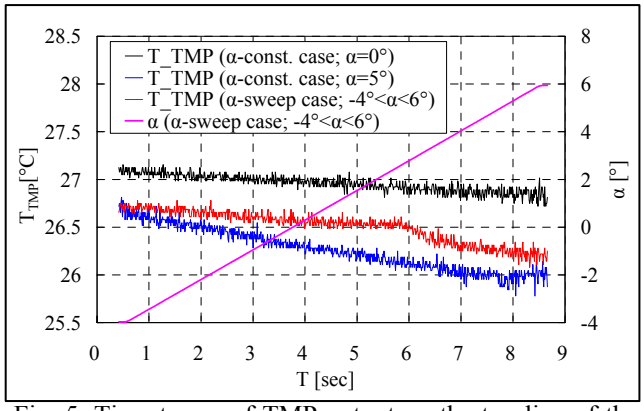

Fig. 5. Time traces of TMP output on the top line of the Sears-Haack body measured in the wind tunnel test.

Figure 6 shows the variations of the local total pressures P_{Pr} measured by Preston tube on the wind tunnel test. Preston tubes mounted different distance from the tip X_{tip}. With increasing angles of attack, the transition location on the top of the model moves to forward. Therefore, the sensor that was located more forward will be measured the laminar flow during the width range of α than the sensor that was located more rearward location. The abrupt change of the pressure observed at α=2~3° on the Preston tube located X_{tip}=250mm was generated by the boundary layer transition. On α<2° the flow is laminar at a sensor location, then the Preston tube measures low pressure than turbulent regions. When the angles of

attack increase within laminar region, the boundary layer developed with the angle of attack, therefore measured pressure by Preston tube decrease because height of Preston tube is constant.

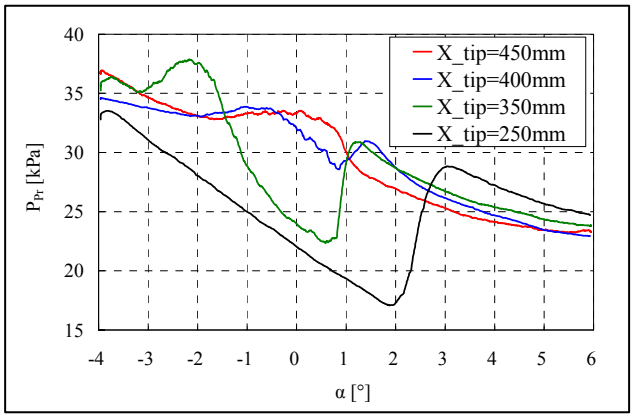

Fig. 6. Variation of local total pressure measured by Pr with angle of attack, and corresponding time traces on the top line of the Sears-Haack body measured in the wind tunnel test.

Since it was confirmed, from the wind tunnel test, that the transition location can be detected in the supersonic boundary layer using four kinds of sensors, the output levels at laminar and turbulent states for HF and DP can be estimated. As mentioned above, the unit Reynolds number and pressure fluctuation in the uniform flow is expected to close to the flight condition and the sensitivity for those quantities is not clear, we estimate that those value obtained in the wind tunnel test is almost same as those obtained in the flight test. By the way, the amplitude of HF AC output seemed too small against to the full range of signal processor (±5V) and that of DP DC output seems too large to the full range of signal processor (almost ±0.11kPa). To modify those to the appropriate value, the gains of HF AC output and DP DC output were changed to 60 times and 140 times respectively for the flight test. In results, the output levels of each sensor at the laminar, turbulent and transitional states in the flight test condition were estimated and summarized in Table 1. The average of HF DC output in the flight test, however, was expected to be lower than that in the wind tunnel test, because the resistance of the sensors mounted on the NEXST-1 is lower than that of the sensors used in the wind tunnel test. Furthermore the HF DC output possibly decreases more, because the surface temperature of the NEXST-1 can rise up to 100°C due to aerodynamic heating. According to this decrease, the fluctuation in HF AC output can also decrease. The effect of circumference temperature, however, could not be predicted quantitatively because of uncertainty about the temperature.

The uncertainty of the pressure coefficient measured from Preston tube was obtained from the pressure measurement system of the NEXST-1 [16]. The uncertainty due to pressure response delay by tubing was also added to the overall uncertainty. The estimated overall uncertainty of the pressure coefficient C_P is less than ±0.0115 at 100:1 odds. A number of checks were conducted to complete high reliability pressure measurement system before and after the flight test.

Table 1. Output level of laminar, turbulent and transition state obtained from wind tunnel test.

	Output at laminar state	Output at transition state (peak value)	Output at turbulent state
E_{MEAN} [V]	3.73	---	3.85
e'_{RMS} [V]	0.03	0.80	0.1-0,4
p'_{RMS} [kPa]	0.011	0.109	0.018

3.2 Other Ground Tests

The other tests to examine the functions of instruments were performed on the ground. Actual accuracy of DP AC output was checked by absorbing pressure from the each sensor directly. From a number of measurements, it was confirmed to be 6.7Pa$_{RMS}$, which corresponds to the 1bit.

Functions of all instruments and electromagnetic interference were tested in the condition that all of them were mounted on the NEXST-1. All data acquired through these tests were analyzed every time to find the abnormal output as early as possible and all four sensors were confirmed in the normal condition even just before the launch.

4 Results of the Flight Experiment

4.1 Transition Measurements

The results of the transition measurement are shown in the following, although the data obtained from the thermocouples is now analyzing and will be presented in other paper.

4.1.1 Hot-Film sensor

The time-series data obtained from the HF was analyzed as follows. First of all, an instantaneous time trace corresponding to each flight test event was taken down, and its characteristics were considered. Secondly, a spectrum was obtained by the FFT analysis. Data with 4096 points were taken down, with 1024 point shift, and these spectrums were averaged 16 times. Then the time average, RMS value, skewness, and maximum and minimum value for each 0.4 seconds were obtained, in order to evaluate the statistical variation in outputs. In the following, our attention is paid to the time-averaged DC output and the RMS value of AC outputs.

First of all, to detect transition location, let us consider the variation in average of the DC output and fluctuation in the AC output at chordwise position normalized by the local chord length X/C=0.25 and Y/S=0.31 in the α–sweep test phase are shown in Fig. 7 as typical results. Variations in lift coefficient C_L are also plotted in the same figure to give a clear comparison between HF output and the flight condition of the NEXST-1 by the sweep of angle of attack. The average HF DC output increased steeply from E_{MEAN}=3.54V to E_{MEAN}=3.59V, at the time from the liftoff T_{LO}=105sec., when the α–sweep test phase began and lift coefficient was C_L=-0.01. It then decreased rapidly to almost the same value as at the beginning E_{MEAN}=3.55V, at T_{LO}=118sec., when the flight condition changed from the 3rd step of the α–sweep test phase (C_L=0.07) to the 4th step of C_L=0.10. Then, thirdly, it began to gradually increase at T_{LO}=123sec., when the flight condition changed from the 4th step to 5th step of C_L=0.14, and overshot when the lift coefficient settled at the 5th step. Finally, at the 6th step (C_L=0.17), the average of the HF DC output settled at E_{MEAN}=3.61V, almost the same value as the 1st to the 3rd steps. As already mentioned, the average of the HF DC output is known to be low in the laminar region, and high in the turbulent region. And such variations have been confirmed in the wind tunnel test. Consequently, the boundary layer at the location is considered to be laminar at the 4th step of C_L= 0.10, turbulent from the 1st step to the 3rd step and at the 6th step, and a transitional state between laminar and turbulent at the 5th step.

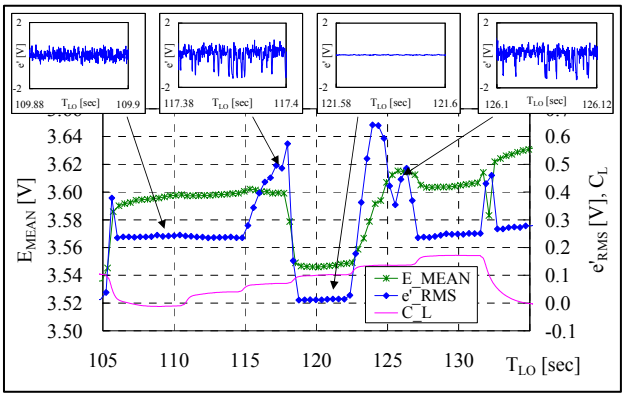

Fig. 7. Variation of HF DC and AC outputs with angle of attack, and corresponding time traces in the flight test.

The fluctuations was very small in e'_{RMS}≈0.02V at the 4th step of the α–sweep test phase between T_{LO}=119sec. and 122sec., when the boundary layer is interpreted as being laminar from the HF DC output. And the fluctuations were very large before and after the 4th step when it corresponds to the 3rd and 5th step. The fluctuations at the 1st, 2nd and 6th steps settled at the comparatively large value e'_{RMS}≈0.24V. These variations correspond closely to the variation from laminar to turbulent observed in the wind tunnel test. Therefore the boundary layer is supposed to be laminar at the 4th step, turbulent at the 1st, 2nd and 6th step and in a transitional state at the 3rd and 5th step. The variation of the state of boundary layer, inferred from the fluctuations in the HF AC output, agrees with that inferred from the average of the HF DC output, qualitatively. Inconsistency is, however, observed at the 3rd step in the strict sense. The boundary layer is inferred to be turbulent from

the HF DC output average, but it is inferred to be in a transitional state from the fluctuations in HF AC output.

To confirm the state of the boundary layer, supposed from the average HF DC output and the fluctuations in HF AC output, instantaneous time trace and spectrum must also be examined. The time trace during 0.03 sec., when the flight condition settles at typical step, is shown in the same figure. The time traces of the 1st, 2nd and 6th step seemed resemble each other, and to be random noise. On the other hand, at the 3rd and 5th steps, a spike signal was observed. These time traces are evidence of the fact that the boundary layer is under a transitional state near turbulent, as confirmed from the wind tunnel test. Then, at the 4th step, the amplitude of the time trace was very small and shows that the boundary layer is laminar. These facts are also clear from the spectrum. As a conclusion, the state of boundary layer which is clarified from the time trace is confirmed to coincide with the state interpreted from the average HF DC output and the fluctuation in HF AC output.

4.1.2 Dynamic Pressure Transducer

Next, let us consider the fluctuating output of DP. As already mentioned, our attention is paid only to the AC outputs. The data was analyzed in the same manner as HF.

From the wind tunnel test as mentioned above, it was confirmed that fluctuations in DP AC output varied coinciding with the HF AC output. The variation of the fluctuation in DP AC outputs shown in Fig. 8 seems to be similar to the fluctuations in HF AC output shown in Fig. 7 at first glance. At X/C=0.20, the fluctuation at the 4th and 5th step was also very small and the boundary layer is interpreted to be in a laminar state. Though the fluctuation in DP AC output was large with p'_{RMS}≈0.02kPa in another condition, which is from the 1st to 3rd step and at the 6th step, the boundary layer at the 2nd and 3rd step is supposed to be under the transitional state. And at the 1st and 6th step, it is supposed to be in a turbulent state for the following reason; the fluctuation on the 2nd and 3rd steps was slightly larger than that on the 1st and 6th steps, and a very large peak was observed at T_{LO}=115sec. between the 2nd and 3rd steps, as well as on the wind tunnel test. A similar peak was also observed at T_{LO}=127sec. between the 5th and 6th steps, though the amplitude was relatively small.

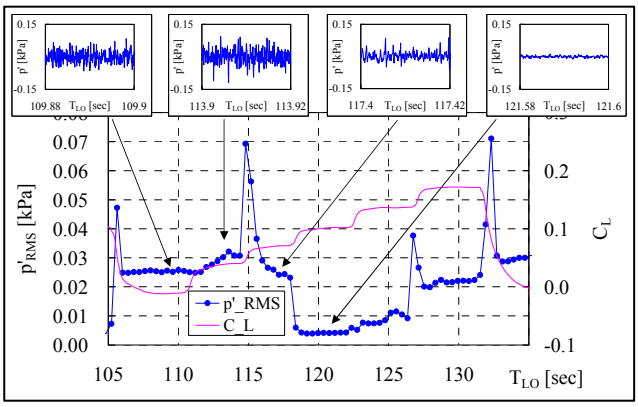

Fig. 8. Variation of DP AC output with angle of attack, and corresponding time traces in the flight test.

The instantaneous time traces at X/C=0.20 are examined to confirm the state of the boundary layer which is inferred from the fluctuations in DP AC output, in the same way as the HF outputs, as shown in the same figure. The characteristics of the time traces from the 1st to 3rd and at the 6th steps, and those at the 4th and 5th steps, resemble each other. Firstly, the time traces of the 4th and 5th step are compared. The amplitude of the 5th step was found to be larger than that of the 4th step. Although there was a difference in the amplitude, the amplitude in the high frequency spectrum component decreased with frequency, and the boundary layer is confirmed to be under a laminar state for both conditions. Next, the time traces from the 1st to 3rd and at the 6th steps are compared. At the 2nd step, the downward spike signals were occurred, although the amplitude was much smaller than that of the HF output. On the other hand, upward spikes were occurred at the 3rd step. And no spike signal was observed at the 1st and 6th steps. Therefore, from the fluctuations it can be concluded that the boundary layer is under a transitional state at the 2nd and 3rd steps, and is under a turbulent state at the 1st and 6th steps.

4.1.3 Preston Tube

Figure 9 shows the variations of the pressure coefficients C_p on α–sweep phase measured by Preston tube at different locations, with the variation of C_L. C_p is defined as the difference between the local total pressure measured by Pr and the static pressure of freestream normalized by the dynamic pressure of freestream.

The C_p at X/C=0.24, Y/S=0.75 (blue line) shows relatively low pressure value during α–sweep test phase as compared with the C_p at X/C =0.50, Y/S =0.20 (red line). The results mean that the flow at X/C =0.24, Y/S =0.75 was laminar, whereas the flow at X/C =0.50, Y/S =0.20 was turbulent. The C_p at X/C =0.37, Y/S =0.39 (green line) was obtained low value at the 4th step on the α–sweep that is the design point, high value at other steps. It was means that the laminar flow was realized at the design point and the transition locations move to forward at other steps. The C_p behaviors were similar with the wind tunnel test results (Fig. 6). It was cleared that the boundary layer transition locations can be detected by Preston tube.

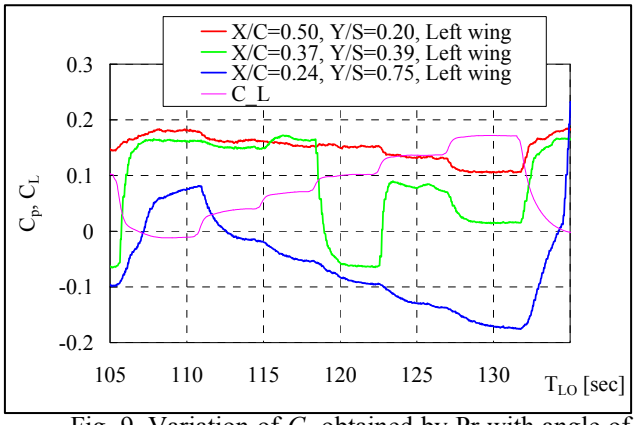

Fig. 9. Variation of C_p obtained by Pr with angle of attack, and corresponding time traces in the flight test.

4.2 Validation of Natural Laminar Flow Wing Concept

The transition location distributions are defined at the end of transition according to objective criteria [20]. Those at the 2nd and 4th steps of the α–sweep test phase, and Re–sweep test phase, are shown in Fig. 10 as a typical case. It is clear that the transition location at the 4th step of the α–sweep test phase (Fig. 10(b)) at C_L=0.10 is much further downstream than the location at the 2nd step (Fig. 10(a)) at C_L=0.04, and that the natural laminar flow effect appears on the wing. Furthermore, the transition location of the Re–sweep test phase is compared with the α–sweep test phase, with the same lift coefficient C_L=0.10 at the design point. Since the altitude of H=12.1 km in the Re–sweep test phase at T_{LO}=167sec. is much lower than that of H=18.1 km in the 4th step of the α–sweep test phase, the corresponding Reynolds number based on the mean aerodynamic chord, Re_c=34.7×10^6 in the Re–sweep test phase is higher than that of Re_c=14.0×10^6 in the α–sweep test phase. As a result, the transition location moves much further forward. From this result, the natural laminar flow effect at the design point (namely, C_L=0.1 at M=2.0 and H=18 km) is obvious (Fig. 10(c)).

It is confirmed that this suppression of transition is caused by the achievement of target surface pressure distribution from the results in the flight test [16,17]. The surface pressure distribution is in good agreement with the CFD results, including the effects of aeroelastical deformation, revision related to the angle of sweep and so on to simulate the flight condition exactly [21]. There observed a steep increasing at the leading edge of the pressure distribution, on the upper surface at the design point, 4th step of the α–sweep test phase. That means the growth of cross-flow instability is suppressed. And following gradual increasing to the trailing edge was observed. That means there observed no adverse pressure gradient region and T-S wave type instability was also suppressed. On the other hand, at the off-design point, for example 2nd step of the α–sweep test phase, though the favorable pressure gradient region was quite narrow, adverse pressure gradient region follows it. Therefore T-S wave type instability is not supposed to be suppressed sufficiently. Since the natural laminar flow effect was confirmed from the experimental data, the effect was then compared with the numerical prediction [3]. The iso-N value line, which was predicted by the LSTAB explained

in Section 1, is also plotted in Fig. 10. The CFD calculation of the boundary layer profile was based on the surface pressure distribution measured during the flight test [16,17]. However, if the iso-N value line appeared in the downstream region after X/C=0.6, we assumed that the amplification of the disturbance was fixed at X/C=0.6 in the transition prediction, because it was not practically easy to maintain the laminar boundary layer after X/C=0.6 due to the existence of the control surface. When the transition location obtained experimentally and numerically were compared, the experimental location was found to be in good agreement with iso-N value line at N=12.5 on the inner wing region of Y/S≤0.6 in all cases, including these three. This N-value was smaller than the specific value of N=14 obtained through the wind tunnel in NASA [22]. Although remarkable discrepancies were observed in the outer wing region, their causes have not been clarified yet. As one of present conclusions, the transition location detected experimentally can be qualitatively at least determined in good agreement with the numerical prediction, based on accordance in the inner wing region.

5 Concluding Remarks

Flight test of a supersonic experimental airplane "NEXST-1" was successfully performed by Japan Aerospace Exploration Agency to validate advanced aerodynamic design technology. To verify the natural laminar flow wing concept, high quality transition measurement system was constructed. By use of these system, the valuable experimental data obtained in the supersonic flight test. The variation in signals corresponding to the laminar-to-turbulent transition process was observed in transition measurements. According to the objective criteria, the state of the boundary layer at each sensor location was classified, and the transition location distribution was obtained for each time. The natural laminar flow effect was confirmed at the design point C_L=0.10, where the transition location moved much further downstream than the off-design point C_L=0.04.

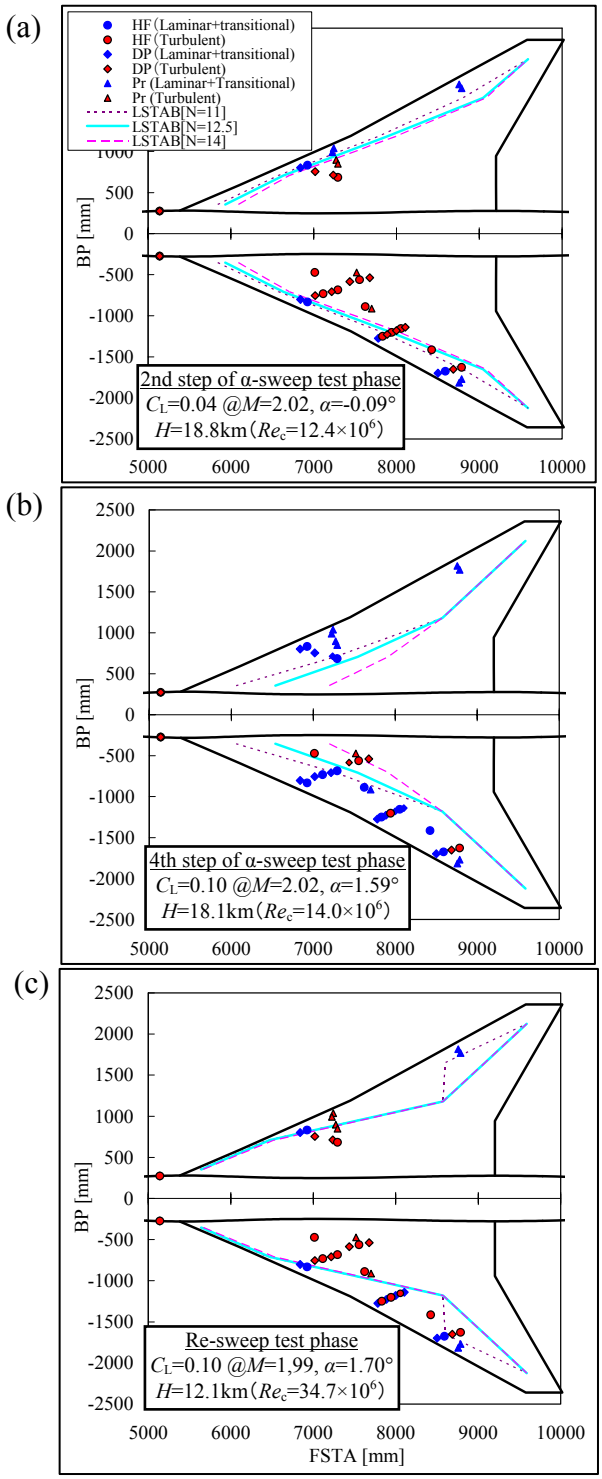

Fig. 10. Transition location distribution. Comparison with "transition level" obtained from experimental result and numerically predicted N-value.

Acknowledgements

The authors are deeply indebted to the staff of Mitsubishi Heavy Industries, Ltd., Kawasaki Heavy Industries, Ltd., Kyowa Electronic Instruments Co. Ltd., and Fuji Heavy Industries, Ltd, for the great efforts they made in making the flight test a success and in obtaining aerodynamic measurements. They would also like to acknowledge the assistance and support for data analysis from Mr. M. Noguchi, Dr. Y. Yokokawa, Mr. Y. Ueda, Dr. T. Fujiwara, Mr. H. Ishikawa, Mr. K. Nakahata, Mr. H. Hirano, Dr. H. Kawakami, Dr. T. Takatoya, and Mr. F. Kuroda, and the advice for instruments from Dr. R. Yanagi of JAXA.

References

[1] Sakata, K., "Supersonic Experimental Airplane (NEXST) for Next Generation SST Technology – Development and Flight Test Plan fir the Unmanned Scaled Supersonic Glider -", *AIAA Paper* 2002-0527, 2002.

[2] Ohnuki, T., Hirako, K., and Sakata, K., "National Experimental Supersonic Transport Project," ICAS 2006-1.4.1, on CD-ROM 2006.

[3] Yoshida, K., and Makino, Y., "Aerodynamic Design of Unmanned and Scaled Supersonic Experimental Airplane in Japan," ECCOMAS 2004, Jyväskylä/Finland, July, 2004.

[4] Carlson H. W., and Miller, D. S., "Numerical Method fot the Design and Analysis of Wings at Supersonic Speeds," NASA TN D7713, 1974.

[5] Kuchemann F. R. S., *The Aerodynamic Design of Aircraft*, Pergamon Press, 1978.

[6] Ashley H., and Landahl, M., *Aerodynamics of Wings and Bodies*, Dover Publications Inc., 1965.

[7] Yoshida K., "Overview of NAL's Program Including the Aerodynamic Design of the Scaled Supersonic Airplane," held at the VKI, RTO Educational Notes 4, 15.1-16, 1998.

[8] Ogoshi, H., "Taerodynamic Design of a Supersonic Airplane Wing – Application of the Natural Laminar Flow Concept to Airfoil," *Proceedings of the 47th Natural Congress of Theoretical & Applied Mechanics,* January, 1988. (in Japanese)

[9] Jeong, S., Matsushima, K., Iwamiya, T., Obayashi, S., and Nakahashi, K., "Inverse Design Method for Wings of Supersonic Transport," *AIAA Paper* 98-0602, 1998.

[10] Arnal D., "Boundary Layer Transition Prediction based on Linear Theory," AGARD Report, No. 793, 1993.

[11] Yoshida, K., Ishida, Y., Noguchi, M., Ogoshi, H., and Inagaki, K., "Experimental and Numerical Analysis of Laminar Flow Control at Mach 1.4," *AIAA Paper* 99-3655, 1999.

[12] Ueda. Y., Ishikawa, H., and Yoshida, K., "Three Dimensional Boundary Layer Transition Analysis in Supersonic Flow Using a Navier-Stokes Code," *Proceedings of ICAS 2004-2.8.2*, on CD-ROM, 2004.

[13] Sugiura, H., Yoshida, K., Tokugawa, N., Takagi, S., and Nishizawa, "Transition Measurements on the Natural Laminar Flow Wing at Mach 2," A., *Journal of Aircraft*, Vol. 39, No. 6, pp. 996-1002, 2002.

[14] Fujiwara, T., Hirako, K., and Ohnuki, T., "Flight Plan and Flight Test Results of Experimental SST Vehicle NEXST-1," ICAS 2006-6.2.1, on CD-ROM 2006.

[15] Yoshida K., Makino, Y., and Shimbo, Y, "An Experimental Study on Unmanned Scaled Supersonic Experimental Airplane," *AIAA Paper* 2002-2842, 2002.

[16] Kwak, D.-Y., Yoshida, K., Ishikwa, H. and Noguchi, M., "Flight Test Measurements of Surface Pressure on Unmanned Scaled Supersonic Experimental Airplane," *AIAA Paper* 2006-3483, 2006.

[17] Kwak, D.-Y., Yoshida, K. and Noguchi, M., "Surface Pressure Measurement System for the Flight Test on Supersonic Experimental Airplane (NEXST-1)," *Proceedings of the 37th JSASS Annual Meeting*, pp.175-178, 2006 (in Japanese).

[18] Owen, F. K., Horstman, C., C., Stainback, P., C. and Wagner, R., D., "Comparison of Wind Tunnel Transition and Freestream Disturbance Measurements," *AIAA Journal*, Vol. 13, No. 3, pp. 266- 269, 1975.

[19] Nishioka, M., Iida, S. And Ichikawa, Y.,**,** "An experimental investigation of the stability of plane Poissuille flow," *Journal of Fluid Mechanics*, Vol. 72, No. 4, , pp. 731-751 1975.

[20] Tokugawa, N., and Yoshida, K., "Transition Detection on Supersonic Natural Laminar Flow Wing in the Flight", *AIAA Paper* 2006-3165, 2006.

[21] Yoshida, K., Kwak, D.–Y., Tokugawa and N., Makino, Y,. "Supersonic Experimental Airplane (NEXST-1) – Aerodynamics and Measurement System Design -", *Proceedings of the 37th JSASS Annual Meeting*, pp.42-45, 2006 (in Japanese).

[22] Joslin, R. D., "Aircraft Laminar Flow Control," *Annual Review of Fluid Mechanics*, Vol. 30, pp. 1-20, 1998.